Hindawi Publishing Corporation
International Journal of Geophysics
Volume 2015, Article ID 806834, 9 pages
http://dx.doi.org/10.1155/2015/806834

Research Article

Acoustic-Gravity Waves Interacting with a Rectangular Trench

Usama Kadri

Department of Mechanical Engineering, Massachusetts Institute of Technology, Cambridge, MA 02139, USA

Correspondence should be addressed to Usama Kadri; ukadri@mit.edu

Received 3 September 2014; Revised 10 December 2014; Accepted 10 December 2014

Academic Editor: Robert Tenzer

A mathematical solution of the two-dimensional linear problem of an acoustic-gravity wave interacting with a rectangular trench, in a compressible ocean, is presented. Expressions for the flow field on both sides of the trench are derived. The dynamic bottom pressure produced by the acoustic-gravity waves on both sides of the trench is measurable, though on the transmission side it decreases with the trench depth. A successful recording of the bottom pressures could assist in the early detection of tsunami.

1. Introduction

The aim of the current work is to study the behaviour of acoustic-gravity waves interacting with a rectangular trench. Acoustic-gravity waves may form in the ocean from various sources, for example, submarine earthquakes, landslides, fall of meteors, underwater explosions, or nonlinear wave interaction. The mathematical formulation of the problem requires accounting for the compressibility of the ocean in order to obtain propagating wave modes other than the gravity mode (i.e., acoustic-gravity modes).

The problems of the diffraction of incident waves by finite obstacles have been extensively examined in the last decades. Amongst these, a problem of interest is the propagation of incident water waves over a trench. Kreisel [1], Mei and Black [2], Lee and Ayer [3], Miles [4], and Kirby and Dalrymple [5] have all investigated water wave diffraction in an incompressible fluid. Ignoring the slight compressibility of ocean results in a single propagating wave mode—the gravity mode. The fluid mechanics significance of the compressibility of the ocean has been investigated by a number of researchers. Among those, Miyoshi [6] investigated the effect of ocean bottom dislocation and showed that as a consequence the surface oscillates up and down; Sells [7] studied the problem of an infinite-strip block in a compressible ocean which undergoes a sudden change and concluded that two types of waves, acoustic and gravity, are generated each dominating distinct space-time regions; Kajiura [8] presented a formula to compute tsunami waves that were generated by a broad crustal deformation using the long wave approximation; Yamamoto [9] carried out an analytical study of the time harmonic problem of the propagation of acoustic and gravity waves in the ocean by vertical oscillation of a block of ocean floor of simplified geometry; Nosov [10] carried out a comparative study of wave generation by piston bottom displacements in compressible and incompressible fluids using linear potential theory; Nosov and Kolesov [11] performed spectrum analysis of bottom pressure variations and proved the existence of elastic oscillations of water column; Chierici et al. [12] modelled the propagation of the generated acoustic signal and tsunami wave generated and included a porous seabed; Renzi and Dias [13] studied the generation of hydroacoustic waves by space-time localised pressure changes on the ocean surface; Kadri and Stiassnie [14] studied the interaction of the generated acoustic modes with the shelf-break; shoaling effects were studied by Kadri and Stiassnie [15], and the contribution of an elastic seafloor was studied by Eyov et al. [16]; Kadri and Stiassnie [17] proved the existence of resonating triad interactions between gravity and acoustic waves which is a main factor in generating microseisms; the importance of triad interaction has been explained in a comprehensive paper by Ardhuin and Herbers [18]; Kozdon and Dunham [19] modelled seismic and acoustic waves from the 2011 Tohoku earthquake and showed that near-trench seafloor uplift excites leaking P waves; and Kadri [20] gave a general solution for the nonlinear interaction of two opposing gravity waves with an acoustic wave in a compressible ocean.

The work by Yamamoto [9] provides an analytical solution of the problem of gravity and acoustic-gravity waves generated by vertical oscillation of a block of ocean floor. Further investigation of the acoustic-gravity waves has been carried out by Kadri and Stiassnie [14], who studied the interaction of acoustic-gravity waves with a continental shelf-break, in order to estimate the dynamic bottom pressure on the reflection and transmission sides of the break. Kadri and Stiassnie [14] constructed separate solutions for each constant depth in terms of eigenfunction expansions of the velocity potential and then matched the solutions at the vertical boundaries resulting in a system of infinite linear algebraic equations with infinite unknowns that is truncated and solved. A similar approach is carried out, in this paper, to formulate and solve the two-dimensional mathematical problem of an acoustic-gravity wave mode, referred to as an incident wave mode, interacting with a rectangular trench in a compressible fluid. We then extend the problem and solve for an incident group of acoustic-gravity wave modes generated by a sudden rise of a block of the ocean floor. As the modes approach a trench, part of the energy is reflected whereas the other part is transmitted. The general solution of the problem enables us to obtain an expression for the dynamic bottom pressure, at the two sides of the trench.

The formulation of the mathematical problem is introduced in Section 2. The solution of a single incident wave is provided in Section 3. A numerical example of a single incident mode interacting with a symmetric trench and solution validation using energy flux balance are presented in Section 4. A second example considering an asymmetric trench is given in Section 5. A third example of a group of incident modes propagating towards a trench is given in Section 6. Finally, concluding remarks are given in Section 7.

2. Formulation and Basics

2.1. Formulation. This paper considers the two-dimensional problem of a wave mode propagating in an ideal homogeneous compressible fluid, with constant frequency ω, over a bottom with a right-angled rectangular trench, as presented in Figure 1 ($h_1 < h_2$ and ($h_3 < h_2$)). As the wave mode interacts with the trench, part of the energy is reflected, whereas the other part is transmitted. The objective is to find the surface wave elevation $z = \eta(x,t)$, as well as the dynamic bottom pressure p_b on the two sides of the trench. To this end, we solve the problem for the flow velocity potential $\phi(x,z,t)$. The governing equation is the two-dimensional wave equation:

$$\phi_{tt} - c^2(\phi_{xx} + \phi_{zz}) = 0, \quad \text{on } -h \le z \le 0, \tag{1}$$

where c is the speed of sound (it is easy to show that variations in the speed of sound in the ocean have a negligible effect on acoustic-gravity waves), $h = h_1$ for $x < 0$, $h = h_2$ for $0 < x < L$, and $h = h_3$ for $x > L$, where L is the trench width.

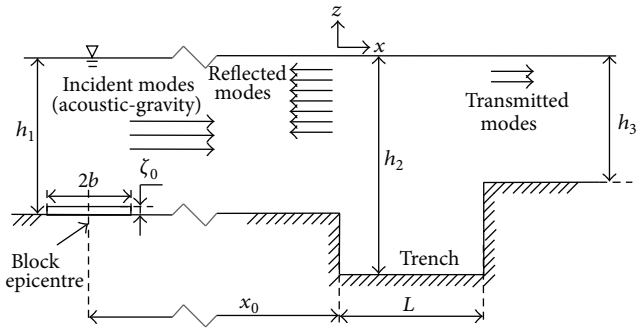

FIGURE 1: Schematic representation of the flow domain; h_1 and h_3 are the depths of the ocean at the two sides of the trench; h_2 and L are the depth and width of the trench, respectively; $2b$ and ζ_0 are the lateral and vertical extents of the bottom motion; x_0 is the distance between the earthquake epicentre and the incidence side of the trench.

Subscripts denote partial derivatives. The bottom and the combined free-surface boundary conditions are, respectively,

$$\phi_z = 0, \quad \text{on } z = -h, \tag{2}$$

$$\phi_{tt} + g\phi_z = 0, \quad \text{on } z = 0, \tag{3}$$

where g is the acceleration due to gravity and h is uniform in each section. The lateral boundary conditions include *Sommerfield*'s radiation condition at $|x| \to \infty$, and

$$\phi_x = 0 \quad \text{on} \begin{cases} x = 0, & -h_2 < z < -h_1 \\ x = L, & -h_2 < z < -h_3. \end{cases} \tag{4}$$

The free-surface elevation and the bottom pressure are then given by

$$\eta(x,t) = -\frac{1}{g}\phi_t, \quad \text{on } z = 0, \tag{5}$$

$$p_b(x,t) = -\rho\phi_t, \quad \text{on } z = -h, \tag{6}$$

where ρ is the density of water.

2.2. Basics. A solution of the linear problem is found by using the method of separation of variables. For any amplitude α_n and a prescribed frequency ω we have the basic solutions

$$\phi_n = \alpha_n f_n(z) e^{i(k_n x - \omega t)}, \quad n = 0, 1, 2, \ldots, \tag{7}$$

where from (1) to (3)

$$f_n(z) = \frac{\cosh[\lambda_n(h+z)]}{\sqrt{I_n}} \tag{8}$$

are the orthonormal eigenfunctions of the *Sturm-Liouville* problem in $z \in (-h, 0)$, with

$$I_n = \int_{-h}^{0} \cosh^2[\lambda_n(h+z)]\,dz; \tag{9}$$

and λ_n are the eigenvalues, which are solutions of the dispersion relation

$$\omega^2 = g\lambda_n \tanh(\lambda_n h). \tag{10}$$

The wave numbers k_n, in (7), are given by

$$k_n^2 = \lambda_n^2 + \frac{\omega^2}{c^2}. \tag{11}$$

The first eigenvalue λ_0, which corresponds to the surface wave, is real, whereas all the rest are purely imaginary. Similarly, the first wave number k_0 is always real. The following $N_{\text{a.g.}}$ wave numbers, $[k_1, k_2, \ldots, k_{N_{\text{a.g.}}}]$, where $N_{\text{a.g.}}$ is the nearest integer smaller than $[\omega h/\pi c + 1/2]$, are also real and are called acoustic-gravity (or hydroacoustic) waves. The gravity and the acoustic-gravity modes are all progressive waves. The remaining wave numbers $[k_{N_{\text{a.g.}}+1}, k_{N_{\text{a.g.}}+2}, \ldots]$ are all imaginary and correspond to decaying evanescent modes.

3. Solution for a Single Incident Wave

Since acoustic-gravity waves are nonevanescent periodic modes (no dissipation is considered, etc.), the width L affects only the evanescent modes, $n > N_{\text{a.g.}}$, which decay exponentially with distance and have a negligible contribution, even in the near-field prior to decaying (see Kadri and Stiassnie [14]). Although the behaviour of acoustic-gravity wave within the trench is of great significance to various applications, for example, deep water transport (see Kadri [21]), the focus here is merely on examining the magnitudes of reflected and transmitted acoustic-gravity wave modes for applications far from the trench, serving, among others, as early precursors of tsunami and rogue waves. Therefore, although we derive expressions for the modes both outside and within the trench, we present results only for modes that are reflected from the incident side of the trench (left side) and those successfully passing the trench (transmitted to the right side).

The solution at the incidence side of the trench (left side), denoted by (1), is given by the incident wave mode, denoted by $\hat{\imath}$ (with $\alpha_{\hat{\imath}} = 1$), propagating to the right, from $x \to -\infty$ to $x = 0$, and an infinite sum of all modes which propagate to the left, from $x = 0$ to $x \to -\infty$, including the evanescent modes that decay exponentially in space:

$$\begin{aligned}\Phi^{(1)} = {} & \frac{\cosh\left[\lambda_{\hat{\imath}}^{(1)}(h_1 + z)\right]}{\sqrt{I_{\hat{\imath}}^{(1)}}} e^{i(k_{\hat{\imath}}^{(1)}x - \omega t)} \\ & + \sum_{n=0}^{\infty} \alpha_n^{(1)} \frac{\cosh\left[\lambda_n^{(1)}(h_1 + z)\right]}{\sqrt{I_n^{(1)}}} e^{-i(k_n^{(1)}x + \omega t)}.\end{aligned} \tag{12}$$

The solution inside the trench, denoted by (2), is given as an infinite sum of all modes which propagate to the right, from $x = 0$ to $x = L$, and an infinite sum of all modes which propagate to the left, from $x = L$ to $x = 0$; in both cases the solution includes the evanescent modes:

$$\begin{aligned}\Phi^{(2)} = {} & \sum_{n=0}^{\infty} \alpha_n^{(2)} \frac{\cosh\left[\lambda_n^{(2)}(h_2 + z)\right]}{\sqrt{I_n^{(2)}}} e^{i(k_n^{(2)}x - \omega t)} \\ & + \sum_{n=0}^{\infty} \widetilde{\alpha}_n^{(2)} \frac{\cosh\left[\widetilde{\lambda}_n^{(2)}(h_2 + z)\right]}{\sqrt{\widetilde{I}_n^{(2)}}} e^{-i[\widetilde{k}_n^{(2)}(x-L) + \omega t]},\end{aligned} \tag{13}$$

where $\widetilde{\lambda}_n^{(2)} = \lambda_n^{(2)}$, $\widetilde{k}_n^{(2)} = k_n^{(2)}$, and $\widetilde{I}_n^{(2)} = I_n^{(2)}$.

The solution in the transmission side of the trench (right side), denoted by (3), is given as an infinite sum of all modes which propagate to the right, from $x = L$ to $x \to \infty$, again including the evanescent modes that here decay exponentially for $x \to \infty$:

$$\Phi^{(3)} = \sum_{n=0}^{\infty} \alpha_n^{(3)} \frac{\cosh\left[\lambda_n^{(3)}(h_3 + z)\right]}{\sqrt{I_n^{(3)}}} e^{i[k_n^{(3)}(x-L) - \omega t]}. \tag{14}$$

From (5), the corresponding surface wave elevations are

$$\begin{aligned}\eta^{(1)} = {} & -\frac{i\omega}{g} \frac{\cosh\left(\lambda_{\hat{\imath}}^{(1)} h_1\right)}{\sqrt{I_{\hat{\imath}}^{(1)}}} e^{i(k_{\hat{\imath}}^{(1)}x - \omega t)} \\ & - \frac{i\omega}{g} \sum_{n=0}^{\infty} \alpha_n^{(1)} \frac{\cosh\left(\lambda_n^{(1)} h_1\right)}{\sqrt{I_n^{(1)}}} e^{-i(k_n^{(1)}x + \omega t)}, \\ \eta^{(2)} = {} & -\frac{i\omega}{g} \\ & \cdot \sum_{n=0}^{\infty} \frac{\cosh\left(\lambda_n^{(2)} h_2\right)}{\sqrt{I_n^{(2)}}} \\ & \cdot \left(\alpha_n^{(2)} e^{i(k_n^{(2)}x - \omega t)} + \widetilde{\alpha}_n^{(2)} e^{-i[k_n^{(2)}(x-L) - \omega t]}\right), \\ \eta^{(3)} = {} & -\frac{i\omega}{g} \sum_{n=0}^{\infty} \alpha_n^{(3)} \frac{\cosh\left(\lambda_n^{(3)} h_3\right)}{\sqrt{I_n^{(2)}}} e^{i(k_n^{(3)}(x-L) - \omega t)}.\end{aligned} \tag{15}$$

The corresponding free-surface amplitudes are given by

$$a_n^{(j)} = \frac{\omega}{g} \left|\alpha_n^{(j)}\right| \frac{\cosh\left(\lambda_n^{(j)} h_j\right)}{\sqrt{I_n^{(j)}}}. \tag{16}$$

The amplitudes of the potentials $\alpha_n^{(1)}$, $\alpha_n^{(2)}$, $\widetilde{\alpha}_n^{(2)}$, and $\alpha_n^{(3)}$ are unknowns, which are found from the following matching conditions (given by Kirby and Dalrymple [5] for water waves):

$$\Phi^{(1)} = \Phi^{(2)}, \quad \text{for } x = 0,\ -h_1 < z < 0,$$

$$\Phi^{(2)} = \Phi^{(3)}, \quad \text{for } x = L,\ -h_3 < z < 0,$$

$$\frac{\partial \Phi^{(1)}}{\partial x} = \begin{cases} 0, & \text{for } x = 0,\ -h_2 < z < -h_1 \\ \dfrac{\partial \Phi^{(2)}}{\partial x}, & \text{for } x = 0,\ -h_2 < z < 0, \end{cases}$$

$$\frac{\partial \Phi^{(2)}}{\partial x} = \begin{cases} 0, & \text{for } x = L,\ -h_2 < z < -h_3 \\ \dfrac{\partial \Phi^{(3)}}{\partial x}, & \text{for } x = L,\ -h_2 < z < 0. \end{cases} \tag{17}$$

Substituting (12)–(14) into (17) and using the orthonormal identity of the eigenfunctions $f_n^{(1)}(z)$ in $z \in (-h_1, 0)$ and $f_n^{(2)}(z)$ in $z \in (-h_2, 0)$ (see (8) and (9)) yield

$$J_{\hat{\imath},M}^{(12)} + \sum_{q=0}^{\infty} J_{q,M}^{(12)} \alpha_q^{(1)} = \alpha_M^{(2)} + \tilde{\alpha}_M^{(2)}, \quad M = 0, 1, 2, \ldots, \tag{18}$$

$$ik_{\hat{\imath}}^{(1)} \delta_{\hat{\imath},M} - ik_M^{(1)} \alpha_M^{(1)} = \sum_{m=0}^{\infty} ik_m^{(2)} J_{M,m}^{(12)} \left(\alpha_m^{(2)} - \tilde{\alpha}_m^{(2)}\right), \quad M = 0, 1, 2, \ldots, \tag{19}$$

$$\sum_{n=0}^{\infty} J_{n,M}^{(23)} \left(\alpha_n^{(2)} + \tilde{\alpha}_n^{(2)}\right) = \alpha_M^{(3)}, \quad M = 0, 1, 2, \ldots, \tag{20}$$

$$ik_m^{(2)} \left(\alpha_M^{(2)} - \tilde{\alpha}_M^{(2)}\right) = \sum_{r=0}^{\infty} ik_r^{(3)} J_{M,r}^{(23)} \alpha_r^{(3)}, \quad M = 0, 1, 2, \ldots, \tag{21}$$

where $\delta_{\hat{\imath},M}$ is the *Kronecker delta,* and

$$J_{n,m}^{(ij)} = \int_{-\min\{h_i, h_j\}}^{0} \frac{\cosh\left[\lambda_n^{(i)}\left(h_i + z\right)\right] \cosh\left[\lambda_m^{(j)}\left(h_j + z\right)\right]}{\sqrt{I_n^{(i)} I_m^{(j)}}} dz. \tag{22}$$

Dividing (19) and (21) by i and substituting $(\alpha_M^{(2)} + \tilde{\alpha}_M^{(2)})$ from (18) into (20) and substituting $(\alpha_M^{(2)} - \tilde{\alpha}_M^{(2)})$ from (19) into (21) give

$$\alpha_M^{(3)} = \sum_{n=0}^{\infty} J_{\hat{\imath},n}^{(12)} J_{n,M}^{(23)} + \sum_{n=0}^{\infty} \sum_{q=0}^{\infty} J_{q,n}^{(12)} J_{n,M}^{(23)} \alpha_q^{(1)}, \quad M = 0, 1, 2, \ldots, \tag{23}$$

$$k_{\hat{\imath}}^{(1)} \delta_{\hat{\imath},M} - k_M^{(1)} \alpha_M^{(1)} = \sum_{m=0}^{\infty} \sum_{r=0}^{\infty} k_r^{(3)} J_{m,r}^{(23)} J_{M,m}^{(12)} \alpha_r^{(3)}, \quad M = 0, 1, 2, \ldots. \tag{24}$$

Finally, substituting $\alpha_M^{(3)}$ from (23) into (24) yields

$$k_M^{(1)} \alpha_M^{(1)} + \sum_{m=0}^{\infty} \sum_{r=0}^{\infty} \sum_{n=0}^{\infty} \sum_{q=0}^{\infty} k_r^{(3)} J_{m,r}^{(23)} J_{M,m}^{(12)} J_{n,r}^{(23)} J_{q,n}^{(12)} \alpha_q^{(1)} = k_{\hat{\imath}}^{(1)} \delta_{\hat{\imath},M} - \sum_{m=0}^{\infty} \sum_{r=0}^{\infty} \sum_{n=0}^{\infty} k_r^{(3)} J_{m,r}^{(23)} J_{M,m}^{(12)} J_{\hat{\imath},n}^{(12)} J_{n,r}^{(23)}, \quad M = 0, 1, 2, \ldots. \tag{25}$$

Equation (25) is a system of infinite linear algebraic equations with infinite unknowns $\alpha_M^{(1)}$. This system of equations can be written in a matrix form and truncated to $\mu + 1$ equations with $\mu + 1$ unknowns as follows:

$$\underbrace{\begin{pmatrix} G_{0,0} + k_0^{(1)} & G_{0,1} & \cdots & G_{0,\mu} \\ G_{1,0} & G_{1,1} + k_1^{(1)} & \cdots & G_{1,\mu} \\ \vdots & \vdots & \ddots & \vdots \\ G_{\hat{\imath},0} & \ddots & G_{\hat{\imath},\hat{\imath}} + k_{\hat{\imath}}^{(1)} & \vdots \\ \vdots & \vdots & \ddots & \vdots \\ G_{\mu,0} & G_{\mu,1} & \cdots & G_{\mu,\mu} \end{pmatrix}}_{\mathbb{A}} \times \underbrace{\begin{pmatrix} \alpha_0^{(1)} \\ \alpha_1^{(1)} \\ \vdots \\ \alpha_{\hat{\imath}}^{(1)} \\ \vdots \\ \alpha_\mu^{(1)} \end{pmatrix}}_{\boldsymbol{\alpha}^{(1)}} = \underbrace{\begin{pmatrix} F_0 \\ F_1 \\ \vdots \\ k_{\hat{\imath}}^{(1)} + F_{\hat{\imath}} \\ \vdots \\ F_\mu \end{pmatrix}}_{\mathbf{B}}, \tag{26}$$

where

$$G_{M,m} = \sum_{m=0}^{\infty} \sum_{r=0}^{\infty} \sum_{n=0}^{\infty} \sum_{q=0}^{\infty} k_3^{(3)} J_{M,r}^{(23)} J_{M,m}^{(12)} J_{n,r}^{(23)} J_{q,n}^{(12)}, \quad M = 0, 1, \ldots, \mu,$$

$$F_M = \sum_{m=0}^{\infty} \sum_{r=0}^{\infty} \sum_{n=0}^{\infty} k_r^{(3)} J_{M,r}^{(23)} J_{M,m}^{(12)} J_{\hat{\imath},n}^{(12)} J_{n,r}^{(23)}, \quad M = 0, 1, \ldots, \mu. \tag{27}$$

Once the matrix $\mathbb{A}$ and the vector $\mathbf{B}$ are calculated, the amplitude of the velocity potential on the left side of the step, $\boldsymbol{\alpha}^{(1)}$, is found from (26):

$$\boldsymbol{\alpha}^{(1)} = \mathbb{A}^{-1} \mathbf{B}. \tag{28}$$

Once $\boldsymbol{\alpha}^{(1)}$ is found, the unknown amplitude vector $\boldsymbol{\alpha}^{(3)}$ (related to the right side of the trench) is obtained from (23).

The reflection and transmission coefficients are, respectively, defined (note that this definition differs from the common definition for surface waves) as

$$K_n^{(R)} \equiv \left|\alpha_n^{(1)}\right|,$$
$$K_n^{(T)} \equiv \left|\alpha_n^{(3)}\right| \frac{\cosh\left[\lambda_n^{(3)} h_3\right]}{\cosh\left[\lambda_n^{(1)} h_1\right]}. \tag{29}$$

4. Numerical Example I: A Single Incident Mode (Validation)

Consider a single acoustic-gravity mode propagating at a prescribed frequency $\omega = 10$ rad/sec and interacting with a rectangular trench, where $h_1 = h_3$ and $h_1 \leq h_2 \leq 3h_1$. The acceleration due to gravity is taken as $g = 10\,\mathrm{m/s^2}$, and the water density is assumed $\rho = 1000\,\mathrm{kg/m^3}$. Following Yamamoto [9] one can show that the average energy flux of the progressive modes is given by

$$\mathbb{F}_n^{(j)} = \frac{1}{2}\rho\omega k_n^{(j)} \left|\alpha_n^{(j)}\right|^2, \quad n = 0, 1, \ldots, N_{\text{a.g.}}. \tag{30}$$

Since the energy flux of each incident mode is either reflected or transmitted, the calculation error, $\mathrm{err}_{\hat{\imath}}$ (of each incident mode), could be estimated by the flux balance

$$\mathrm{err}_{\hat{\imath}} = 1 - \frac{\sum \mathbb{F}_n^{(1)} + \sum \mathbb{F}_n^{(3)}}{\mathbb{F}_{\hat{\imath}}^{(1)}}, \quad \text{for } n = 0, 1, \ldots, N_{\text{a.g.}}, \tag{31}$$

where $\mathbb{F}_{\hat{\imath}}$ is the energy flux of the incident mode and $\mathbb{F}_n^{(1)}$ and $\mathbb{F}_n^{(3)}$ are the corresponding energy fluxes of the reflected and transmitted modes, respectively. Note that all computations consider at least the first 19 modes ($\mu \leq 19$), which include the zero mode (gravity wave), acoustic-gravity, and evanescent modes. Nevertheless, we only present results for acoustic-gravity waves.

Figure 2 presents calculations of $K^{(R)}$ and $K^{(T)}$, which represent the reflection (see left column subplots) and transmission (see right column subplots) coefficients, for the first eight incident modes, as function of trench depth ratio h_2/h_1. In each subplot, the bold number indicates the incident mode (e.g., in the third row the incident mode is $\hat{\imath} = 3$) and the bold curve is the reflection or transmission in the same mode as of the incident ($n = \hat{\imath}$). Figure 2 predicts, as expected, zero reflection and full transmission of energy by the incident mode at the absence of a trench ($h_2/h_1 = 1$). More interestingly, it shows that at $h_2/h_1 > 1$ the energy is primarily transferred to the mode of incidence as well as to the neighbouring modes. However, as the trench depth increases most of the reflected energy is transferred to the mode of incidence, while most of the transmitted energy is transferred to the leading modes, in particular to the first mode. It is also noticeable that the magnitude of transmission, for all modes, is oscillatory and dependent on the trench depth.

In order to assess the accuracy of the calculations presented in Figure 2 we use the energy flux balance which is given in (31). The energy flux of the incident mode prior to interacting with the trench is equal to the sum of energy fluxes of all reflected and transmitted modes as given in (31). In all cases the error $\mathrm{err}_{\hat{\imath}}$ is enormously small $O(10^{-14})$, which is a validation of the flux conservation assumption.

5. Numerical Example II: Asymmetric Trench

This section examines the effect of trench asymmetry on the reflection and transmission coefficients. Consider a similar problem as described in example II though with $h_1 = 4000$ m, $h_2 = 7000$ m, and $500 \leq h_3 \leq 7000$ m. Figure 3 presents calculations of $K^{(T)}$ (upper subplot) and $K^{(R)}$ (lower subplot), for the leading incident acoustic-gravity mode, as function of trench asymmetry ratio h_3/h_1. The bold number indicates the leading incident mode ($\hat{\imath} = 1$). Figure 3 predicts, as expected, that as h_3/h_1 increases, the transmission coefficient of the leading mode increases, while the reflection coefficient decreases, and vice versa. Interestingly, as h_3 increases more modes arise, each having locally a maximum $K^{(T)}$ at about $h = 3\pi(n-1)c/\omega$, $n = 2, 3, \ldots$. Note that $h_3/h_1 = 1$ predicts the same coefficients given in Figure 2 (upper subplots), for the same trench relative depth, that is, $h_2/h_1 = 1.75$.

6. Numerical Example III: A Group of Incident Modes

In this section we consider a group of N incident acoustic-gravity modes, generated by a rise of a block of the ocean floor propagating towards a trench as shown in Figure 1. In the current example, the depth of the ocean at the two sides of the trench is $h_1 = h_3 = 4000$ m, and the trench depth is $h_2 = 11000$ m. The distance between the block epicentre and the left side of the trench is $x_0 = 10^6$ m. The speed of sound in water is $c = 1500$ m/s. Following Nosov [10] the motion of the bottom is given by

$$\frac{\partial \zeta(x,t)}{\partial t} = \frac{\zeta_0}{\tau} \mathscr{H}\left(b^2 - \left(x + x_0\right)^2\right) \mathscr{H}[t(\tau - t)], \tag{32}$$

where the function $\mathscr{H}$ is the Heaviside function; $\zeta_0 = 1$ m, $b = 4 \times 10^4$ m, and $\tau = 10$ s are the vertical and the lateral extents and the duration of the bottom motion, respectively. Note that, apart from the bottom motion due to the block movement, the bottom is assumed rigid. Following Stiassnie [22], the incident acoustic-gravity modes at $(0, t_0)$ propagate each at a specific frequency given by

$$\omega_{\hat{\imath}} = \frac{-i\lambda_{\hat{\imath}}^{(1)} c}{\sqrt{1 - \left(x_0/ct_0\right)^2}}, \tag{33}$$

where $\lambda_{\hat{\imath}}^{\prime(1)}$ is real ($\lambda_{\hat{\imath}}^{(1)} = i\lambda_{\hat{\imath}}^{\prime(1)}$). For a group of N incident modes, each propagating with its own frequency $\omega_{\hat{\imath}}$, the total

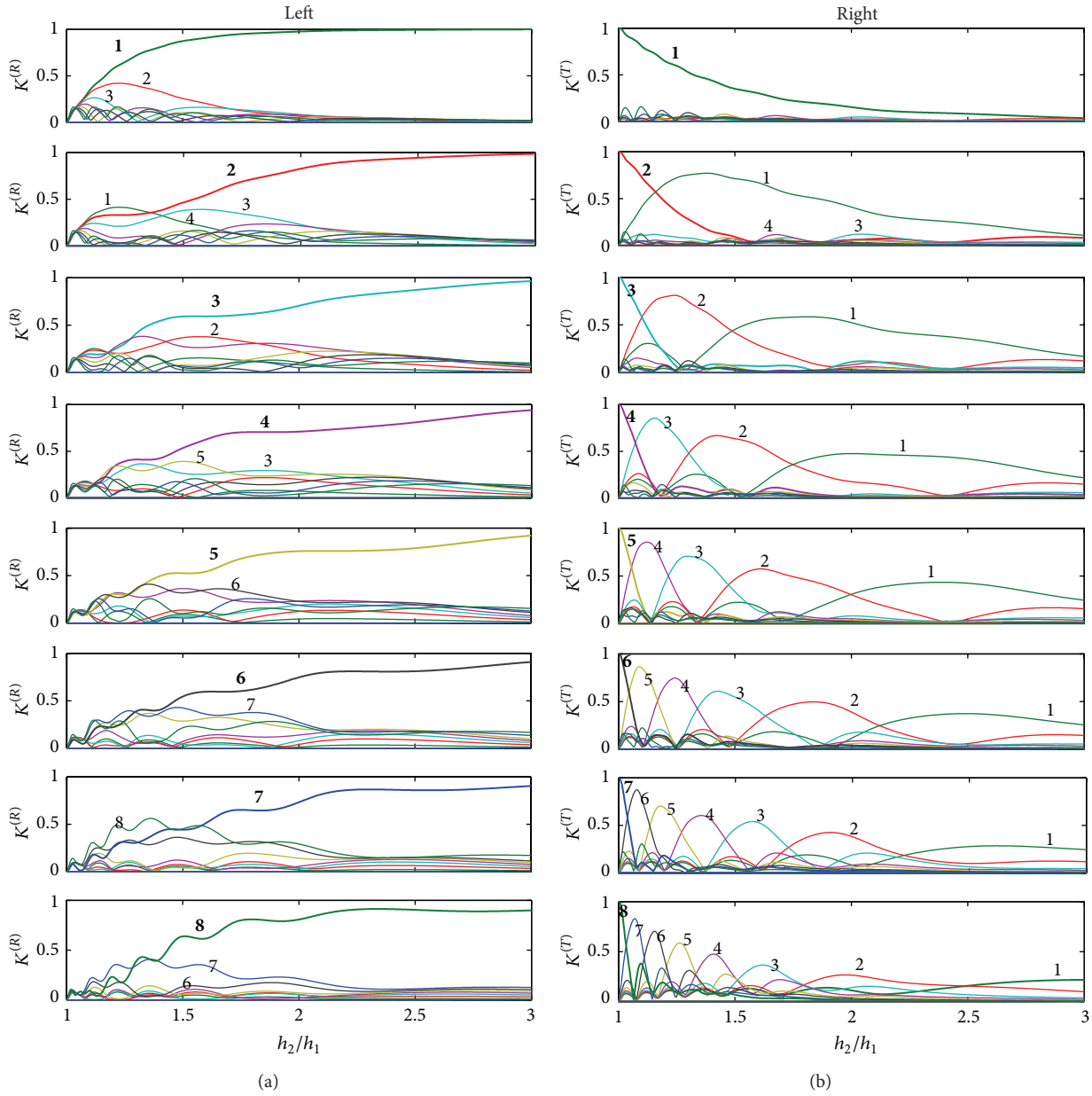

FIGURE 2: Reflection and transmission of amplitude coefficients on the left ($K^{(R)}$) and right ($K^{(T)}$) sides of a rectangular trench as function of the trench depth h_2/h_1. The ocean depth on the two sides of the trench is $h_1 = h_3 = 4000$ m. In each subplot, the bold number indicates the mode of incidence $\hat{\imath}$. The calculation error, $\mathrm{err}_{\hat{\imath}} \ll 10^{-14}$.

velocity potential on the jth side of the trench caused by all incident modes is

$$\Phi^{(j)} = \sum_{\hat{\imath}=1}^{N} \beta_{\hat{\imath}}^{(1)} \Phi_{\hat{\imath}}^{(j)}(\omega_{\hat{\imath}}), \tag{34}$$

where $\Phi_{\hat{\imath}}^{(j)}(\omega)$ is the velocity potential on the jth side of the trench caused by the $\hat{\imath}$th incident mode. Since the considered problem is linear, each $\Phi_{\hat{\imath}}^{(j)}(\omega)$ ($\hat{\imath} = 1, 2, \ldots, N$) is solved separately based on the solution given in Section 3. The $\beta_{\hat{\imath}}^{(1)}$ are the complex amplitudes of the incident modes that are evaluated from the surface elevation at $(0, t_0)$, given in (28) of Kadri and Stiassnie [14]:

$$\beta_{\hat{\imath}}^{(1)} = -i \frac{g}{\omega_{\hat{\imath}}} \frac{\zeta_0 \sqrt{I_{\hat{\imath}}^{(1)}}}{\cos\left(\lambda_{\hat{\imath}}^{\prime(1)}\right)} \times \frac{2^{5/2} t_0^{1/2} \left(1 - \left(x_0/ct_0\right)^2\right)^{5/4}}{\sqrt{\pi} \left(\lambda_{\hat{\imath}}^{\prime(1)}\right)^{5/2} c^{1/2} \tau x_0 h_1}$$

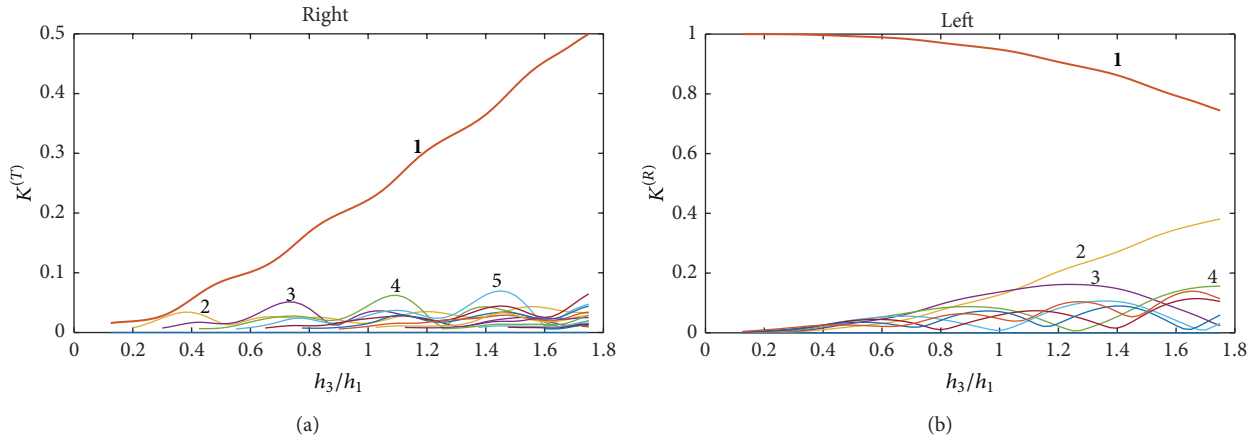

FIGURE 3: Reflection and transmission of amplitude coefficients on the left ($K^{(R)}$) and right ($K^{(T)}$) sides of a rectangular trench of depth $h_2 = 7000$ m. The ocean depth on the left side of the trench is $h_1 = 4000$ m, whereas the depth on the right side of the trench $h_3 = 500 \cdots 7000$ m. The bold numbers indicate the mode of incidence $\hat{\imath} = 1$. The calculation error, $\mathrm{err}_{\hat{\imath}} \ll 10^{-14}$.

$$\times \sin\left(\frac{\lambda_{\hat{\imath}}'^{(1)} c\tau/2}{\sqrt{1-\left(x_0/ct_0\right)^2}}\right) \times \sin\left(\frac{\lambda_{\hat{\imath}}'^{(1)} bx_0/(ct_0)}{\sqrt{1-\left(\tilde{x}/ct_0\right)^2}}\right) \times \exp\left(-i\left(\lambda_{\hat{\imath}}'^{(1)}\sqrt{c^2{t_0}^2-{x_0}^2}+\frac{\pi}{4}\right)\right). \tag{35}$$

The total dynamic bottom pressure caused by all N incident modes is

$$p_b^{(j)} = \sum_{\hat{\imath}=1}^{N} \beta_{\hat{\imath}}^{(1)} p_{b,\hat{\imath}}^{(j)}(\omega_{\hat{\imath}}), \tag{36}$$

where $p_{b,\hat{\imath}}^{(j)}(\omega_{\hat{\imath}})$ is the dynamic bottom pressure caused by the $\hat{\imath}$th incident mode calculated by (6).

Table 1 presents the following values for each incident mode $\hat{\imath}$: frequency $\omega_{\hat{\imath}}$, wave number $k_{\hat{\imath}}$, wavelength $l_{\hat{\imath}}$, and incident wave amplitude $a_{\hat{\imath}}$. For each incident mode $\hat{\imath}$ there are $r = 1, \ldots, \hat{\imath}$ reflected and transmitted modes that all propagate at the same frequency $\omega_{\hat{\imath}}$. Only the $\hat{\imath}$th reflected or transmitted mode has the same wave properties as the incident mode.

Figure 4 presents calculations of the total dynamic bottom pressure at the trench, on its left ($x = -\epsilon$) and right ($x = L + \epsilon$) sides, where $\epsilon \ll 1$. The number of incident acoustic-gravity modes is $N = 8$. The bottom pressure amplitudes on the left and right sides of the trench are 760 Pa (7.5×10^{-3} atm) and 220 Pa (2.2×10^{-3} atm), respectively. Compared to the sensitivity of existing sensors, these magnitudes are sufficiently large for measurement purposes.

Since the amplitudes of the incident modes are oscillatory in both space and time, contributions of higher modes to the dynamic bottom pressure may become significant (the first mode is not necessarily the leading). It is noticeable that as long as the transmission side of the trench is deep enough, to allow for the existence of acoustic-gravity waves, the total pressure will have an oscillatory nonevanescent contribution.

TABLE 1: Values for the first 8 incident modes; $h_1 = 4000$ m, $g = 10$ m/s^2, and $c = 1500$ m/s.

$\hat{\imath}$	$\omega_{\hat{\imath}}$ [rad/s]	$k_{\hat{\imath}}$ [rad/m]	$l_{\hat{\imath}}$ [km]	$a_{\hat{\imath}}$ [m]
1	0.608	8.890×10^{-5}	70.7	5.877×10^{-3}
2	1.824	2.966×10^{-4}	21.2	3.062×10^{-3}
3	3.039	4.982×10^{-4}	12.6	1.919×10^{-3}
4	4.255	6.989×10^{-4}	8.99	1.158×10^{-3}
5	5.471	8.993×10^{-4}	6.99	6.237×10^{-4}
6	6.687	1.099×10^{-3}	5.71	2.758×10^{-4}
7	7.902	1.299×10^{-3}	4.83	8.399×10^{-5}
8	9.118	1.500×10^{-3}	4.19	8.409×10^{-6}

7. Concluding Remarks

The two-dimensional problem of an acoustic-gravity wave mode propagating towards a rectangular trench in an ideal compressible fluid has been addressed. As an incident acoustic-gravity mode reaches the trench, part of the energy is reflected whereas the rest is transmitted. The two parts are distributed among the allowed wave modes. The dynamic bottom pressure is calculated from the potential amplitudes of the transmitted and reflected modes.

Calculations of the total dynamic bottom pressure at both sides of the trench show that although the magnitudes of the bottom pressure on the transmission side of the trench decrease, it is sufficiently large for measuring purposes. Note that the contribution of evanescent modes to the dynamic bottom pressure has been considered by Kadri and Stiassnie [14] who showed that convergence due to the consideration of evanescent modes is relatively fast, and in the present case their contribution is negligible. The contribution of evanescent modes becomes significant when the transmission side

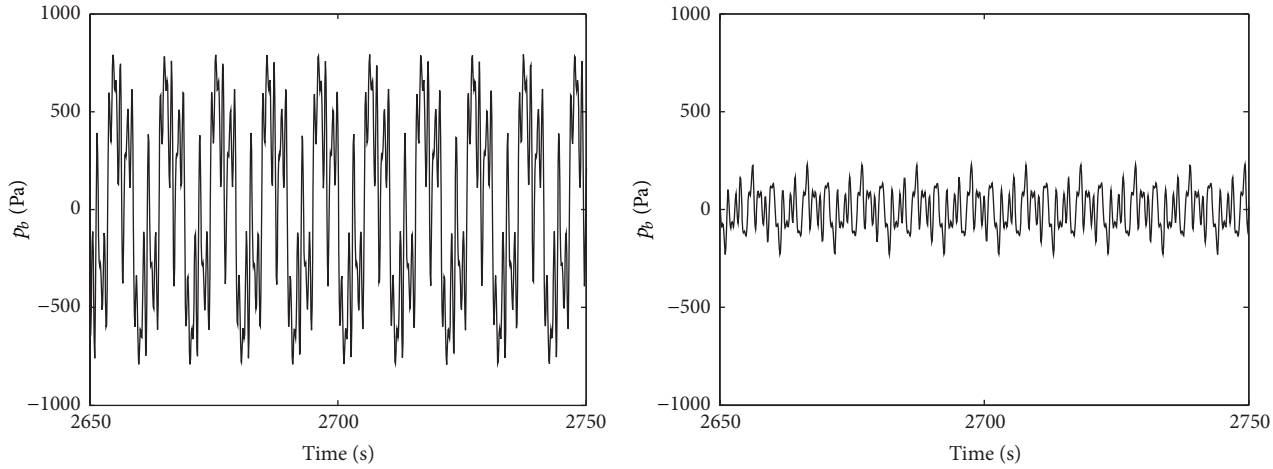

Figure 4: Calculations of the dynamic bottom pressure at both sides of the trench; at $x = -\epsilon$ (a) and $x = L + \epsilon$ (b), where $\epsilon \ll 1$.

of the trench is shallow enough to prevent the existence of the low acoustic-gravity modes.

The results presented here might find application in verifying numerical codes for wave propagation and certain observational studies. However, such an application is bounded by the idealised bathymetry, as mode coupling can be sensitive to ocean floor irregularities, with sharp depth variations; another limitation is the neglect of coupling to the elastic ocean floor. Considering the elasticity of the bottom results in *Rayleigh* waves (e.g., see Stoneley [23]), or *Scholte* type of waves (e.g., see Webb and Shultz [24]), and thus might be important when discussing the properties of waves interacting with the ocean floor at near-critical depths. The transition of acoustic-gravity waves into *Rayleigh* waves at critical depths, and into *Scholte* wave at the shoreline, is thoroughly discussed in Eyov et al. [16]. Moreover, note that the low acoustic-gravity modes have wavelengths larger than to be trapped within the SOFAR channel. Therefore, energy loss due to refraction and scattering on a more realistic and elastic bottom with irregularities has to be considered in order to assess the magnitude of the acoustic-gravity bottom pressure far from the source. If the pressure is still found measurable, it should be considered for the early detection of tsunami as proposed, among others, by Chierici et al. [12] and Kadri and Stiassnie [14].

Conflict of Interests

The author declares that there is no conflict of interests.

References

[1] G. Kreisel, "Surface waves," *Quarterly of Applied Mathematics*, vol. 7, pp. 21–44, 1949.

[2] C. C. Mei and J. L. Black, "Scattering of surface waves by rectangular obstacles in water of finite depth," *Journal of Fluid Mechanics*, vol. 38, no. 3, pp. 499–511, 1969.

[3] J.-J. Lee and R. M. Ayer, "Wave propagation over a rectangular trench," *Journal of Fluid Mechanics*, vol. 110, pp. 335–347, 1981.

[4] J. W. Miles, "On surface-wave diffraction by a trench," *Journal of Fluid Mechanics*, vol. 115, pp. 315–325, 1982.

[5] J. T. Kirby and R. A. Dalrymple, "Propagation of obliquely incident water waves over a trench," *Journal of Fluid Mechanics*, vol. 133, pp. 47–63, 1983.

[6] H. Miyoshi, "Generation of the tsunami in compressible water (part I)," *Journal of the Oceanographical Society of Japan*, vol. 10, pp. 1–9, 1954.

[7] C. C. L. Sells, "The effect of a sudden change in shape of the bottom of a slightly compressible ocean," *Philosophical Transactions for the Royal Society of London, Series A*, vol. 258, no. 1092, pp. 495–528, 1965.

[8] K. Kajiura, "Tsunami source, energy and directivity of wave radiation," *Bulletin of the Earthquake Research Institute*, vol. 48, no. 5, pp. 835–869, 1970.

[9] T. Yamamoto, "Gravity waves and acoustic waves generated by submarine earthquakes," *International Journal of Soil Dynamics and Earthquake Engineering*, vol. 1, no. 2, pp. 75–82, 1982.

[10] M. A. Nosov, "Tsunami generation in compressible ocean," *Physics and Chemistry of the Earth, Part B: Hydrology, Oceans and Atmosphere*, vol. 24, no. 5, pp. 437–441, 1999.

[11] M. A. Nosov and S. V. Kolesov, "Elastic oscillations of water column in the 2003 Tokachi-oki tsunami source: in-situ measurements and 3-D numerical modelling," *Natural Hazards and Earth System Science*, vol. 7, no. 2, pp. 243–249, 2007.

[12] F. Chierici, L. Pignagnoli, and D. Embriaco, "Modeling of the hydroacoustic signal and tsunami wave generated by seafloor motion including a porous seabed," *Journal of Geophysical Research C: Oceans*, vol. 115, no. 3, Article ID C03015, 2010.

[13] E. Renzi and F. Dias, "Hydro-acoustic precursors of gravity waves generated by surface pressure disturbances localized in space and time," *Journal of Fluid Mechanics*, vol. 754, pp. 250–262, 2011.

[14] U. Kadri and M. Stiassnie, "Acoustic-gravity waves interacting with the shelf break," *Journal of Geophysical Research: Oceans*, vol. 117, Article ID C03035, 2012.

[15] U. Kadri and M. Stiassnie, "A note on the shoaling of acoustic-gravity waves," *WSEAS Transactions on Fluid Mechanics*, vol. 8, no. 2, pp. 43–49, 2013.

[16] E. Eyov, A. Klar, U. Kadri, and M. Stiassnie, "Progressive waves in a compressible-ocean with an elastic bottom," *Wave Motion*, vol. 50, no. 5, pp. 929–939, 2013.

[17] U. Kadri and M. Stiassnie, "Generation of an acoustic-gravity wave by two gravity waves, and their subsequent mutual interaction," *Journal of Fluid Mechanics*, vol. 735, pp. R61–R69, 2013.

[18] F. Ardhuin and T. H. C. Herbers, "Noise generation in the solid Earth, oceans and atmosphere, from nonlinear interacting surface gravity waves in finite depth," *Journal of Fluid Mechanics*, vol. 716, pp. 316–348, 2013.

[19] J. E. Kozdon and E. M. Dunham, "Constraining shallow slip and tsunami excitation in megathrust ruptures using seismic and ocean acoustic waves recorded on ocean-bottom sensor networks," *Earth and Planetary Science Letters*, vol. 396, pp. 56–65, 2014.

[20] U. Kadri, "Wave motion in a heavy compressible fluid: revisited," *European Journal of Mechanics—B/Fluids*, vol. 49, part A, pp. 50–57, 2015.

[21] U. Kadri, "Deep ocean water transport by acoustic-gravity waves," *Journal of Geophysical Research*, vol. 119, no. 11, pp. 7925–7930, 2014.

[22] M. Stiassnie, "Tsunamis and acoustic-gravity waves from underwater earthquakes," *Journal of Engineering Mathematics*, vol. 67, no. 1-2, pp. 23–32, 2010.

[23] R. Stoneley, "The effect of the ocean on Rayleigh waves," *Geophysical Journal International*, vol. 1, supplement 7, pp. 349–356, 1926.

[24] S. C. Webb and A. Shultz, "Very low frequency ambient noise at the seafloor under the Beaufort Sea icecap," *Journal of the Acoustical Society of America*, vol. 91, no. 3, pp. 1429–1439, 1992.